IEEE Access
Multidisciplinary | Rapid Review | Open Access Journal

Received March 27, 2019, accepted April 27, 2019. Date of publication xxxx 00, 0000, date of current version xxxx 00, 0000.

Digital Object Identifier 10.1109/ACCESS.2019.2914580

Cable Diagnostics With Power Line Modems for Smart Grid Monitoring

YINJIA HUO[1], (Student Member, IEEE), GAUTHAM PRASAD[1], (Student Member, IEEE), LAZAR ATANACKOVIC[1], LUTZ LAMPE[1], (Senior Member, IEEE), AND VICTOR C. M. LEUNG[1,2], (Fellow, IEEE)

[1]Department of Electrical and Computer Engineering, The University of British Columbia, Vancouver, BC V6T 1Z4, Canada
[2]College of Computer Science and Software Engineering, Shenzhen University, Shenzhen 518060, China

Corresponding author: Lutz Lampe (lampe@ece.ubc.ca)

This work was supported by the Natural Sciences and Engineering Research Council of Canada (NSERC).

ABSTRACT Remote monitoring of electrical cable conditions is an essential characteristic of the next-generation smart grid, which features the ability to consistently surveil and control the grid infrastructure. In this paper, we propose a technique that harnesses power line modems (PLMs) for monitoring cable health. We envisage that all or most of these PLMs have already been deployed for data communication purposes and focus on the distribution grid or neighborhood area networks in the smart grid. For such a setting, we propose a machine learning (ML)-based framework for automatic cable diagnostics by continuously monitoring the cable status to identify, assess, and locate possible degradations. As part of our technique, we also synthesize the state-of-the-art reflectometry methods within the PLMs to extract beneficial features for the effective performance of our proposed ML solution. The simulation results demonstrate the effectiveness of our solution under different aging conditions and varying load configurations. Finally, we reflect on our proposed diagnostics method by evaluating its robustness and comparing it with existing alternatives.

INDEX TERMS Smart grid monitoring, cable diagnostics, aging, power line communications, reflectometry, machine learning.

I. INTRODUCTION

A salient feature of smart grids is ubiquitous monitoring and control targeted for purposes such as frequency regulation, demand response, asset management, and anomaly detection [2]. As a smart grid monitoring technique, cable health monitoring falls into the latter two categories, since underground cables are crucial assets of the grid infrastructure and are widely deployed in both transmission and distribution systems due to their aesthetics, robustness to weather conditions, and reduced impact on the environment [3], [4]. Cable in-service failures lead to severe anomalies such as power outages. An ideal solution to avoid in-service failures in operating cables is to identify potential issues and anticipate faults in a non-destructive manner [5, Ch. 6]. Such a proactive diagnostics approach, however, is known to be challenging as opposed to a reactive solution like hard fault detection [6]. Despite this, various diagnostics schemes have been developed in the past that attempt to identify and locate cable degradations [5, Ch. 6], [7, Ch. 4].

The associate editor coordinating the review of this manuscript and approving it for publication was Alberto Sendin.

A major drawback of the existing cable diagnostics schemes is the requirement of dedicated equipments to conduct the tests [5, Ch. 6], [8]. To counter this, we propose reusing power line modems (PLMs) that are installed in the grid for smart-grid communications purposes [9], [10]. Any two PLMs in the network communicating with each other, regularly estimate the power line communication (PLC) channel condition between them for efficient end-to-end communications. We have shown in our recent works that this estimated channel condition also provides insight into the health of the power cables [1], [11], [12]. PLMs operating with broadband power line communication (BB-PLC) technology use analog-to-digital converters functioning at sampling rates of up to 200 MHz [13]. Signals that are sampled at such high rates provide distinctive information about the deterioration of cable insulation dielectric properties as the cables age and degrade [14], [15, Ch. 2, Ch. 7], [16], [17]. This means that changes in the cable dielectric properties manifest themselves as variations in the BB-PLC channels estimated inside legacy PLMs. This enables us to design a PLM-based proactive diagnostics technique to identify potential issues and anticipate faults along the cable by monitoring

the communication channel conditions. Additionally, this scheme can also operate online, unlike several other conventional methods that require cables to be de-energized during testing [5, Ch. 6].

Another major disadvantage of conventional diagnostics solutions is that most of them require technical staff with expertise to analyze the measured signals (current and/or voltages) and determine the cable health status [5, Ch. 6]. This manual interpretation introduces added costs and slows down the diagnostics procedure. Furthermore, varying network load conditions result in signal changes that are on occasions similar to those caused due to cable degradations. This renders manual diagnosis susceptible to missed detections and false alarms (FAs). To overcome these drawbacks, we propose augmenting our PLM-based approach with machine learning (ML) techniques to intelligently analyze the communication channel conditions estimated by the PLMs, and design a self-reliant and an automated cable diagnostics solution that can be implemented remotely.

A. CONTRIBUTIONS

In this paper, we present for the first time, an ML framework for independent cable diagnostics that builds on PLM signal measurements and applies a multi-step cooperative scheme to progressively detect, assess, and locate possible cable degradations. Our automated solution focuses on first determining the type of degradation that the cable is subject to, whether localized to a portion of the cable or spreading homogeneously across its length. For either type of degradation, we diagnose its severity to preempt a potential cable in-service failure that may occur if a cable beyond the normal service condition is left untreated. For a localized degradation, we further locate its position and the affected length so that remedial efforts can be concentrated at the right location.

To aid the design of our solution, we study the underlying signal propagation principles, develop suitable strategies to extract signal features that are indicative of cable degradations and use those features to infer cable health using appropriate ML algorithms that we choose from existing ML toolboxes. In particular, the performance of our solution relies on the quality of the chosen features. Inspired by state-of-the-art joint-time-frequency domain reflectometry (JTFDR) solutions, which are fairly effective in cable anomaly detection and localization [18], we design features extracted from the JTFDR waveform, together with other features extracted from the estimated communication channel. However, adopting conventional JTFDR requires bulky expensive external devices and experienced technicians to be dispatched onsite, which are not consistent with the target characteristics of our solution that we previously outlined. To overcome this overhead, we devise a method to synthesize JTFDR within the PLMs, called PLM-JTFDR. Thereby, we incorporate PLM-JTFDR as part of our ML diagnostics solution by extracting features from its resultant waveforms.

As part of our solution, we use synthetically generated data for the ML training. For this purpose, we adopt a cable aging model from the literature [19], [20], refine it for faithful emulation of realistic cable degradations, and further apply it to generate the PLC channels using a bottom-up approach. We generate channels under different network loads and cable degradation conditions for extracting features to train our machines. We use a sufficient number of samples while training a machine such that the ML algorithm performance is saturated. We note that since practical operation of our solution involves off-site training, we are not limited by the number of training samples used. For practical implementation, several machines are trained for a variety of diagnostics tasks and are loaded onto the PLMs in the grid through software/firmware upgrades in a remote manner. We also reflect on our solution and contrast it with other state-of-the-art methods, which predominantly have drawbacks that include requiring dedicated diagnostics equipments, demanding manual intervention for performing the tests and analyzing the data, providing insufficient resolution for focused remedial efforts, and/or being unable to predict a future in-service failure caused by an untreated cable degradation.

Further, in order to verify the effectiveness of our schemes, we present a comprehensive simulation-based evaluation of our proposed solution under a generic network topology with varying load conditions and arbitrary cable aging profiles. Further, to judge the effectiveness of our proposed solution under real-world scenarios, we critically evaluate its robustness by emulating non-idealities that could be encountered during practical deployment. In particular, we conduct a robustness and sensitivity analysis of our solution with behavior variations from the adopted degradation models.

B. OUTLINE

The rest of the paper is organized as follows. In Section II, we introduce the modeling of cable degradation, including its growth and the dielectric property change it causes within the insulation. We then describe the modeling and generation of PLC channels subject to a particular degradation condition under a considered network topology in Section III. In Section IV, we introduce our proposed ML framework for automated cable diagnostics, including PLM-JTFDR for feature extraction. We present the simulation results in Section V, and discuss the potential challenges for our proposed solution and compare it with prior works in Section VI. Conclusions are drawn in Section VII. The specifics of PLM-JTFDR and the details of our ML implementation are relegated to the Appendices A-C.

Nomenclature: Throughout this paper, we use $\Re(x)$ and $\Im(x)$ to indicate real and imaginary part of a complex number x, respectively. We denote a uniform random distribution between a and b as $\mathscr{U}(a, b)$.

II. CABLE AGING MODEL

Based on the insulation material used, power cables are classified into laminated and extruded types [5, Ch. 6.2.3]. While laminated cables suffer mainly from thermal degradations, extruded ones are mostly susceptible to electrical

TABLE 1. List of abbreviations.

AdaBoost	Adaptive Boosting
BB-PLC	Broadband Power Line Communications
CFR	Channel Frequency Response
FA	False Alarm
IBFD	In-Band Full-Duplex
JTFDR	Joint-Time-Frequency Domain Reflectometry
L2Boost	Least-square Boosting
LD	Localized Degradation
ML	Machine Learning
MTL	Multi-conductor Transmission Line
MV	Medium Voltage
PLC	Power Line Communications
PLM	Power Line Modem
PMU	Phasor Measurement Unit
PUL	Per-Unit-Length
RBF	Radial Basis Function
SI	Self-Interference
SVM	Support Vector Machine
TDR	Time Domain Reflectometry
TEM	Transverse Electromagnetic
WT	Water Treeing
XLPE	Cross-Linked Polyethylene

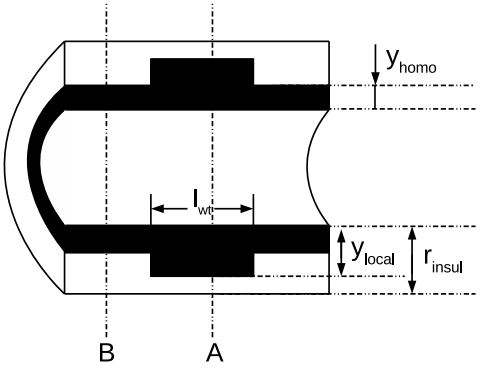

FIGURE 1. Longitudinal section of a cable insulation illustrating the cable aging profile. The shaded region indicates the portion of the insulation subject to WT degradation while the unshaded region consists of the intact sections of the insulation and the conductor-insulation interface.

aging, i.e., developing water-treeing (WT) and electrical-treeing [21]. In this paper, we focus on investigating cable aging caused by WT degradations, since WT is a prominent cause for premature failures of extruded cables [22], [5, Ch. 6]. In addition, focusing on WT degradations has the added benefit that many works in the literature, e.g., [19], [20] have developed a deterministic model for WT growth and thoroughly investigated the dielectric properties of WT-degraded extruded cross-linked polyethylene (XLPE) insulation, which is widely deployed [3], [4], [23].

A. CABLE AGING PROFILE

Investigations into the nature of WT in cable insulations have shown that under normal operating conditions, power cables develop near-uniform WT degradations across their length as they age [17], [19]. However, water ingress or local defects may lead to salient localized WT degradations [19]. Therefore, for faithful emulation, we model the aging condition along the cable with an aging profile as shown in Fig. 1. The cable section develops a homogeneous WT degradation along its length with thickness y_{homo}, within the total insulation thickness of r_{insul}. In addition, a section of the cable, of length ℓ_{WT}, may also be subject to a localized WT degradation of thickness y_{local}.

TABLE 2. Cable ageing model parameters [19], [20], [25], [26, p. 794].

Diffusion constant of water into the dielectric (α_0)	1.44×10^4
Size of the free-volume voids (ν_0)	2.5×10^{-28} m^3
Mains frequency on the line (f_0)	60 Hz
Absolute permittivity (ϵ_0)	8.8×10^{-12} F/m
Relative permittivity of non-degraded XLPE (ϵ_{PE})	$2.3 - 0.001j$
Dielectric mechanical yield strength (Y)	2×10^7 Pa
Depolarization factor (D)	$\frac{1}{12}$
Absolute water content in the WT region (q_w)	0.06
Conductivity of water (σ_w)	0.22 S

The growth of y_{homo} can be related to the elapsed service time, t_{sr}, as [19][1]

$$y_{\mathsf{homo}} = \left(\frac{\alpha_0 \nu_0 f_0 \, F^2 \epsilon_0 \Re\{\epsilon_w\} t_{\mathsf{sr}}^{\frac{3}{2}}}{Y} \right)^{\frac{1}{3}}, \tag{1}$$

where F is the operating electric field strength (see Section III). The remaining parameters are all listed in Table 2 along with their values that we use in our model.[2] Thus, in case of homogeneous aging, an estimated value of y_{homo} can be used to obtain an *equivalent age*, t_{eq}, of a degraded cable, which can be computed as

$$t_{\mathsf{eq}} = \sqrt[3]{\left(\frac{Y \cdot y_{\mathsf{homo}}^3}{\alpha_0 \nu_0 f_0 F^2 \epsilon_0 \Re\{\epsilon_w\}} \right)^2}. \tag{2}$$

This equivalent age provides an intuitive indication into the WT degradation severity that the cable has experienced.

B. DIELECTRIC PROPERTIES OF WT DEGRADED CABLES

The dielectric properties of WT degraded XLPE insulation material have been investigated in the literature, e.g., in [20], [27]. The relative permittivity of WT degraded XLPE insulation (shown as the shaded region in Fig. 1) can be computed as [27, Eq. 1]

$$\epsilon_{\mathsf{WT}} = \epsilon_{\mathsf{PE}} \left(1 + \frac{q_w(\epsilon_w - \epsilon_{\mathsf{PE}})}{D(1 - q_w)(\epsilon_w - \epsilon_{\mathsf{PE}})} \right), \tag{3}$$

where the relative permittivity of water is given by $\epsilon_w = 81 - j\frac{\sigma_w}{2\pi f \epsilon_0}$ for any operating frequency f, where $j = \sqrt{-1}$. Please refer to Table 2 for descriptions and values of all other parameters. For the overall cross section of XLPE insulation with both WT degraded and intact regions, the equivalent relative permittivity can be computed using the series dielectrics model as [20, Eq. 6.3],

$$\epsilon_{\mathsf{total}} = \left(\frac{y}{r_{\mathsf{insul}}} \frac{1}{\epsilon_{\mathsf{WT}}} + \frac{r_{\mathsf{insul}} - y}{r_{\mathsf{insul}}} \frac{1}{\epsilon_{\mathsf{PE}}} \right)^{-1}, \tag{4}$$

where y is the WT degradation depth.

[1]The accuracy of (1) has been validated with real-world measurements in [19].

[2]Note that the properties of XLPE insulation material vary with the manufacturing process and depend on various factors including its density and crystallinity [24]. The parameters listed in Table 2 are values obtained under typical situations and serve as nominal parameters.

To further determine and establish degradation severities, we define $\gamma \triangleq \frac{y}{r_{\text{insul}}}$ as the relative depth of the XLPE insulation that is impacted with the WT degradation. For a cross section with a localized WT degradation (e.g., cross section A in Fig. 1), we have $y = y_{\text{local}}$ and $\gamma_{\text{local}} = \frac{y_{\text{local}}}{r_{\text{insul}}}$. For other cross sections without a localized WT degradation (e.g., cross section B in Fig. 1), we have $y = y_{\text{homo}}$ and $\gamma_{\text{homo}} = \frac{y_{\text{homo}}}{r_{\text{insul}}}$. For an aging profile without any localized WT degradation, we have $\gamma = \gamma_{\text{homo}} = \frac{y_{\text{homo}}}{r_{\text{insul}}}$ along the entire length of the cable segment.

III. PLC CHANNEL MODEL

Our next step involves generating several power line channels for healthy and degraded cables that will be used as training and testing samples in our ML framework. PLC channel modeling is typically addressed either through the top-down or the bottom-up approach. While the top-down approach could be computationally simpler, we adopt the bottom-up approach of modeling PLC channels in this investigation in order to accurately capture the influence of the insulation dielectric property changes resulting from a specific aging profile [28].

For a given aging profile of cable insulation, each segment along the cable with the same degradation severity can be viewed as a uniform line with electrically small cross-sectional dimensions, in which condition PLC signals are transmitted in the quasi-transverse-electromagnetic (quasi-TEM) propagation mode, and the PLC channel can be modeled with the multi-conductor transmission line (MTL) theory [29, Ch. 1]. We then concatenate each of these sections to obtain the overall PLC channel modeling. By using the WT degradation model of (4) in the MTL per-unit-length (PUL) parameter computations specified in Section III-A, we model the PLC channel for cable sections with arbitrary degradation conditions. For the software implementation, we feed the computed PUL parameters to an open source bottom-up PLC channel emulator of [30] to generate PLC channels.

A. COMPUTATION OF PUL PARAMETERS

The MTL theory models the PLC channel with the MTL equations, whose coefficients are determined by the PUL parameters, which contain all cross-sectional information of every cable segment [29, Ch. 1]. Therefore, the first step in MTL analysis is to determine the PUL resistance (**R**), inductance (**L**), capacitance (**C**), and conductance (**G**) matrices. For an N conductor cable with $N \geq 2$, **R**, **L**, **C**, and **G** matrices are all of dimensions $(N-1)\times(N-1)$.

Let us denote the 0th line as the reference conductor. Accordingly, we obtain each of the (i,j)th element of **R** as [29, Eq. 3.12]

$$R_{ij} = R_0 + R_j, \quad i = j, \tag{5}$$
$$R_{ij} = R_0, \quad i \neq j, \tag{6}$$

where R_i is the PUL resistance of the ith conductor ($0 \leq i \leq (N-1)$). Since the surrounding medium of the conductors is typically non-ferromagnetic with permeability of free space, i.e., $\mu = \mu_0 = 4\pi \times 10^{-7}\ \text{H}\cdot\text{m}^{-1}$, and since its permittivity is irrelevant in determining **L**, we apply the wide separation approximations for round conductors in free space to get [29, Eq. 5.23]

$$L_{ij} = \frac{\mu_0}{2\pi} \ln\left(\frac{d_{0,j}^2}{r_0 r_j}\right), \quad i = j, \tag{7}$$
$$L_{ij} = \frac{\mu_0}{2\pi} \ln\left(\frac{d_{0,i} d_{0,j}}{r_0 d_{i,j}}\right), \quad i \neq j, \tag{8}$$

where r_j is the radius for the j-th conductor and $d_{i,j}$ is the separation distance between the ith and jth conductors.

Further, for computational simplicity we can assume a homogeneous surrounding medium with a permittivity of ϵ_{total}. Under such conditions, we compute the capacitance and conductance matrices as [29, Eq. 5.24]

$$\mathbf{C} = \mu_0 \epsilon_0 \Re\left(\epsilon_{\text{total}}\right) \mathbf{L}^{-1}, \tag{9}$$
$$\mathbf{G} = -2\pi f \mu_0 \epsilon_0 \Im(\epsilon_{\text{total}}) \mathbf{L}^{-1}. \tag{10}$$

Note that this simplification only leads to a faster PUL computation and does not affect the operation of our proposed solution. With these PUL parameters, we generate PLC channels under different aging conditions and varying network loads and topologies using the channel generator tool of [30].

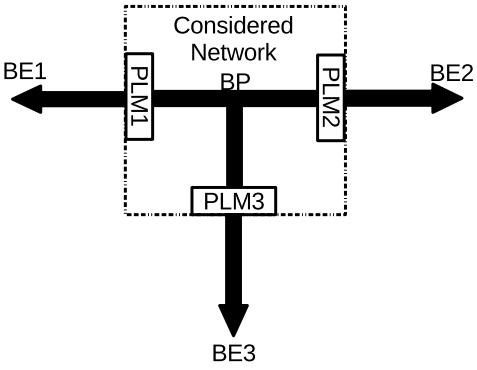

FIGURE 2. Portion of the distribution network considered.

B. NETWORK TOPOLOGY AND LOADS

Along with the knowledge of cable PUL parameters, channel generation also requires information about the network topology and the connected loads. Typical medium voltage (MV) distribution networks consist of few intermediate branches and can be divided into smaller T and chain networks [31]. Therefore, for a realistic grid emulation, we consider a T-network with three PLMs, as shown in Fig. 2, with possible network extensions beyond each of the PLMs. Each of the six branches in the considered network topology assumes an aging profile shown in Fig. 1 with the same γ_{homo}. In addition, a localized WT degradation with γ_{homo} and ℓ_{WT} may be present on any of the six branches or not. Without loss of generality, we consider a symmetrical topology with

an equal separation distance of 500 m between each PLM and the branch point (BP) [32]. Further, we also place a 500 m transmission line between each PLM and any further branch extensions (BEs). To emulate a range of realistic network extensions [33, Table 1.1], at every BE in Fig. 2, we consider equivalent load impedances randomly chosen in $\mathscr{U}(0, 50) + j \cdot \mathscr{U}(-50, 50)\ \Omega$ between each pair of conductors as shown in [12, Fig. 3], where $j = \sqrt{-1}$.

C. CABLE SETTINGS

The final aspect of characterizing the PLC channel is to specify the physical cable parameters. In our evaluations, we consider the XLPE multi-core cable N2XSEY [34], with equidistant conductor separations of $d_{\text{cond}} = 15.88$ mm, equal conductor radii $r_{\text{cond}} = 3.99$ mm and a maximum rated voltage $V_0 = 12$ kV. We then apply an approximate cylindrical geometry to compute the electric field under V_0 at a distance r_{cond} from the center of the conductor [35, Eq. 1], where the electric field strength is at its maximum and is most prone for WT inception [35], as

$$F_{\max} = \frac{V_0}{r_{\text{cond}} \ln\left(\frac{d_{\text{cond}}}{2r_{\text{cond}}}\right)}. \tag{11}$$

Considering an expected maximum service time of $t_{\max} = 30$ years [5, Ch. 6] in (1), we derive the maximum homogeneous degradation severity, $\max(\gamma_{\text{homo}}) = 0.0481$ under nominal conditions shown in Table 2. Therefore, in our evaluations, we confine $\gamma_{\text{homo}} \leq 0.05$, and to clearly distinguish a salient localized WT degradation, we let $\gamma_{\text{local}} \geq 0.1$.

D. PLC CHANNEL GENERATION

We use the PLC channel emulator of [30] to generate PLC channels in the frequency range of $2 - 30$ MHz with a frequency resolution of $\Delta f = 24.414$ kHz. The channel generator of [30] provides the end-to-end channel frequency response (CFR), H_{f}, and the line access impedance, Z_{in}. Using Z_{in} and the known PLM output impedance, we compute the reflection channel transfer function, H_{ref}, which characterizes the behavior of the portion of the transmitted PLC signal that is reflected into the modem [36]. Therefore, in our ML framework, we use both H_{f} and H_{ref} to extract features for the training and the testing. Note that both these channels are inherently estimated within the PLMs in some form, and hence introduces no additional overhead [13], [37]. While H_{f} is directly estimated within all legacy PLMs, Z_{in} or H_{ref} can be obtained in either of two ways. Newer PLMs that support adaptive power boosting, regularly estimate Z_{in} to compute the input return loss [13]. Alternatively, H_{ref} can also be acquired using in-band full-duplex (IBFD) communication functionality which inherently involves estimating the self-interference (SI) channel to cancel the echo [37]. In the context of PLC, the echo/SI channel essentially indicates H_{ref} [37], [38]. In this work, we consider H_{f} and H_{ref} to be perfectly estimated by the PLMs in order to focus specifically on determining the potential of using PLC channel variations to estimate cable degradations.

IV. ML FRAMEWORK FOR CABLE HEALTH MONITORING

In this section, we introduce our proposed ML solution for automated cable diagnostics.

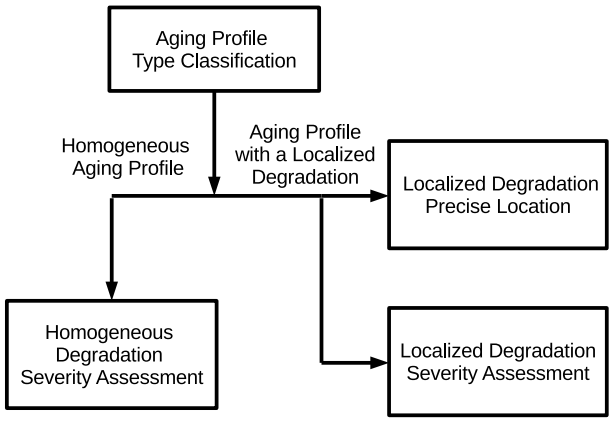

FIGURE 3. Our proposed multi-step cable diagnostics.

A. CABLE HEALTH MONITORING

We conduct the evaluation of cable health conditions through a series of procedures as shown in Fig. 3. In the first stage, we perform an aging profile type classification, where we either detect a localized degradation (LD) or a homogeneous aging profile. When the cable has undergone homogeneous degradation, we assess its degradation severity. The case of a healthy cable is encompassed within this condition when a severity assessment results in zero degradation. In cases where the cable is subject to an LD, we locate this defect and assess its severity.

B. PLM-JTFDR

The state-of-the-art in reflectometry for LD diagnostics is JTFDR, which transmits a reference signal that is customized based on the application, and then conducts advanced post-processing of the received reflected signal before analyzing [18]. While JTFDR shows promising results in cable anomaly detection and location, applying conventional JTFDR in its native form requires external equipments, which incur extra costs, as described in Section I. To overcome this implementation drawback, we propose a new method called PLM-JTFDR, to synthesize the results of JTFDR operation, i.e., to obtain the resultant JTFDR waveform, h_{JTFDR}, within PLMs by using H_{ref}. We describe PLM-JTFDR in greater detail in Appendix A.

Since JTFDR is limited to LD diagnostics due to its nature of operation, we consider PLM-JTFDR for developing parts of our solution focused on detecting, locating, and assessing LDs. An LD causes discontinuities in dielectric properties of cable insulations, which results in parts of the PLC signal to be reflected back to the PLM from the locations

of these discontinuities. By determining the presence and locations of such reflections, which can be noticed as peaks in the PLM-JTFDR waveforms, an LD can be identified and localized.

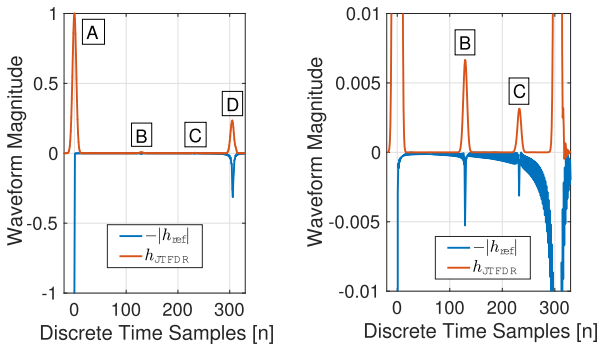

FIGURE 4. (a) h_{JTFDR} and $-|h_{\text{ref}}|$ (normalized to the magnitude of peak A) when a degradation is present between PLM1 and BP. (b) Zoomed at the degradation locations *B* and *C*.

As an example, we study the use of PLM-JTFDR for LD diagnostics under a network topology shown in Fig. 2. We first run PLM-JTFDR with an aging profile that contains an LD located between the transmitting PLM, i.e. TX, and BP. We set the LD to be of the minimum degradation severity, $\gamma_{\text{local}} = 0.1$, to evaluate the sensitivity of our methods to mild degradations. We set an arbitrary degradation length of 166 m to be present between 211 m and 377 m from PLM1 as TX. The resultant waveforms obtained for this setup is shown in Fig. 4.[3] For comparison, we also show $-|h_{\text{ref}}|$ alongside, which is essentially the resultant waveform of conventional time-domain reflectometry (TDR) [39]. We notice from Fig. 4 that h_{JTFDR} is smoother and its peaks are more prominent than for h_{ref}. Therefore, compared to TDR, i.e., directly using h_{ref} for cable diagnostics, PLM-JTFDR has superior sensitivity and performance to detect less salient localized WT degradations. The superior performance of our solution is more prominent when the LD is further away from the measurement point (PLM1), e.g., between PLM2 and BP, as shown by the results in Fig. 5.

The peak locations in Fig. 4 are seen to be at $n_{\text{A}} = 0$, $n_{\text{B}} = 129$, $n_{\text{C}} = 232$, $n_{\text{D}} = 305$. Since the network topology is known *a-priori*, i.e., that BP is $\ell_0 = 500$ m away from PLM1 and that n_{D} indicates the reflection from BP, we can compute the two ends of the LD to be $\ell_0 n_{\text{B}}/n_{\text{D}} = 211$ m and $\ell_0 n_{\text{C}}/n_{\text{D}} = 380$ m apart from PLM1, respectively. While we predict the start location of the degradation accurately, the slight disagreement in locating the degradation end point can be attributed to the slower wave propagation speed in the LD region. For a section of cable with ϵ_{total} (see (4)), the wave

[3]For illustration clarity, we only show the first 330 time samples of the signal, which contains all pertinent reflection peaks. The signal is normalized with respect to the magnitude of its first peak.

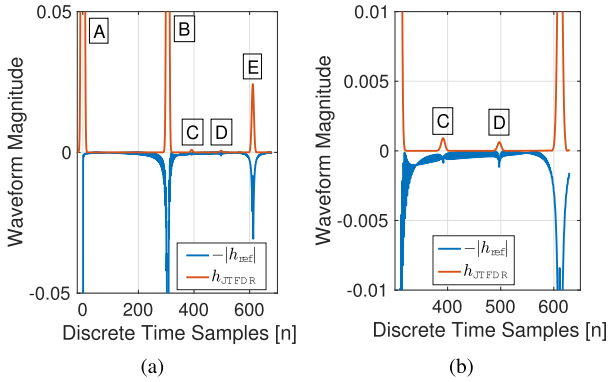

FIGURE 5. (a) h_{JTFDR} and $-|h_{\text{ref}}|$ (normalized to the magnitude of peak A) when a degradation is present between PLM2 and BP. (b) Zoomed at the degradation locations *C* and *D*.

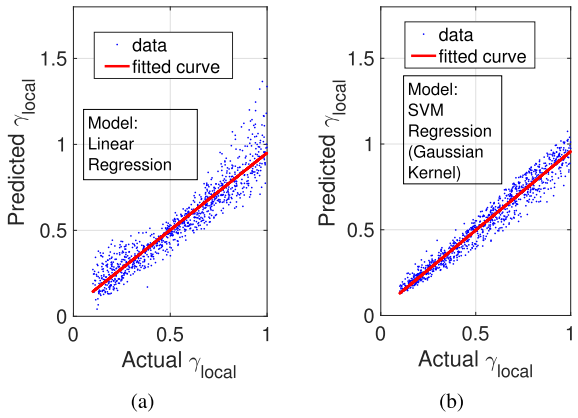

FIGURE 6. Prediction of γ_{local} using peak magnitudes and locations of the PLM-JTFDR waveforms. (a) Linear regression. (b) SVM regression with Gaussian kernel.

propagation velocity can be computed as

$$v = \frac{1}{\sqrt{\mu\epsilon_0 \Re(\epsilon_{\text{total}})}}. \tag{12}$$

When $\gamma_{\text{local}} \gg \gamma_{\text{homo}}$, v at the region with a localized WT degradation is noticeably different from other regions. This is also shown in [11], [20], [40], where fault or degradation localization in severely aged service cables yields significant deviance from their true values.

Our evaluations thus far show the capability of our proposed PLM-JTFDR in identifying and locating an LD. However, this only completes a portion of the LD diagnostics tasks. In the following, we attempt to perform the remaining LD severity estimation by exploiting the principle that a more severe degradation causes stronger discontinuities in cable insulation dielectric properties, and thus results in a higher reflection peak in h_{JTFDR}. Therefore, we monitor the peak amplitudes to infer the extent of degradation. However, we find the relationship between peak amplitudes and the degradation severities to be non-linear, and furthermore affected by signal attenuations along the line and changing load conditions. This can be observed from Fig. 6, where we apply regression techniques in an attempt to predict the

degradation severity level of an LD. We train our machine with 3600 aging profiles using the peak amplitudes and locations as features, and their associated $\gamma_{\text{local}} \sim \mathcal{U}(0.1, 1)$ as labels. Our prediction results for 1000 other aging profiles subject to LD with $\gamma_{\text{local}} \sim \mathcal{U}(0.1, 1)$ is shown in Fig. 6.

We observe in Fig. 6(a) that applying linear regression to predict γ_{local} provides an unsatisfactory prediction performance. On the other hand, the results in Fig. 6(b) are more encouraging, where the performance is improved by using a support vector machine (SVM) regression with the Gaussian kernel. This further motivates us to include the results of PLM-JTFDR in some form within an ML-based cable diagnostics solution.

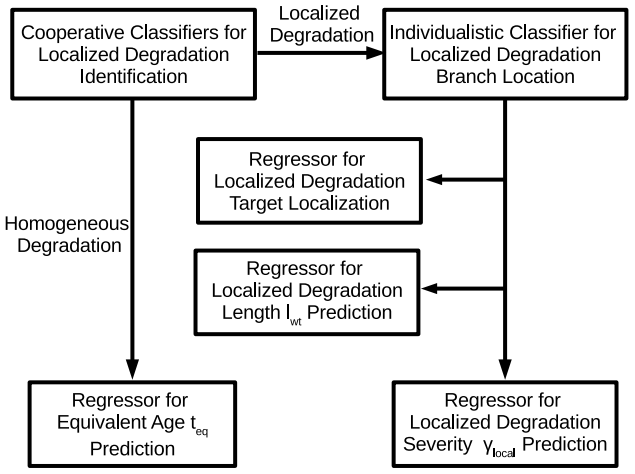

FIGURE 7. Proposed ML framework for cable health monitoring.

C. A MACHINE LEARNING FRAMEWORK

Our proposed ML-based cable diagnostics solution is shown in Fig. 7. We formulate the problems of aging profile type identification and branch location as supervised classification tasks, and the problems of degradation location and aging severity assessment as supervised regression tasks. For each of these supervised learning tasks, we train the machine using features extracted from the synthetically generated channel transfer functions with their associated known aging profiles following the procedure outlined in Section III. In particular, for each of the supervised classification tasks, we use the presence or absence of an LD as the training label/tag. Similarly, for every supervised regression task, we use the value to be predicted, e.g., γ_{homo} and ℓ_{wt}, as shown in Fig. 7, as the training label/tag.

Throughout our analysis, we consider the generic T-network topology of Fig. 2. To determine the presence of an LD, we run classifiers in each of the PLMs to identify an LD in their nearest branch(es). We then employ a cooperative technique, by which we conclude that no LD exists if all of the PLMs report the absence of an LD at their nearest branches. In such a case, the cables are predominantly subject only to homogeneous degradation across the network. On the other hand, when a PLM reports the presence of an LD, we face the challenge of topological ambiguity, where the degradation could be located on a branch in either direction of the PLM.[4] In the network of Fig. 2, when the ith PLM, p_i, reports an LD, the LD can lie either between $p_i - \mathsf{BP}$ or $p_i - \mathsf{BE}_i$. To eliminate this ambiguity, we perform a second round of classification to detect the LD branch location. In the second round, we let p_j ($j \in \{1, 2, 3\}, j \neq i$) confirm whether the degradation resides between p_i and BP using a similar classification procedure. Once the presence of an LD is confirmed within the considered network, we use different ML regressors in the PLM closest to the LD for severity assessment and localization. In particular, we use an ML regressor to find the associated γ_{local}, another one to predict its length, i.e., ℓ_{wt}, and a final one to predict the distance between the PLM and the near-end of the LD, which we also refer to as the *target* location.

On the other hand, when the aging profile is identified to be homogeneous, we use an ML regressor to predict an equivalent cable age, t_{eq}, which provides an intuitive indication into the overall degradation severity of the evaluated cable insulation. Specifically, we train a machine to predict γ_{homo} of the evaluated homogeneous aging profile and use (2) to compute t_{eq} with the nominal cable parameters listed in Table 2.

D. MACHINE LEARNING ALGORITHMS

For both classification and regression, we use two sets of ML techniques, namely SVM and boosting, following their success both in previous cable diagnostics evaluations as well as in other domains [1], [11], [41]. SVM is a classical and popular ML technique, which constructs support vectors of hyperplanes, from a subset of the training data, for predictions. It encodes sparsity in the hinge loss function, which is a convex upper-bound for the non-smooth $0 - 1$ loss function, and results in a small number of support vectors compared to the number of training samples [41, Ch. 14]. The sparsity and the well-known large margin principle allows SVM to provide accurate predictions for unseen data samples. Furthermore, optimization problems in SVM operation can be efficiently solved by convex quadratic programming, and a high-dimensional space can be explored by kernel tricks.

Boosting is one of the meta-ML algorithms that works by consolidating multiple weak learners into a strong learner. It applies the weak learners sequentially to weighted versions of the data, where a higher weight is allocated to examples that suffered greater inaccuracy in earlier prediction rounds [41, Ch. 16]. These weak learners are typically only marginally better than random guessing but are computationally simple. Boosting is also known to be robust to overfitting, and can be efficiently executed since it is a forward stage-wise additive model [41, Ch. 16]. We use the adaptive boosting (AdaBoost) for classification and the gradient

[4]For our evaluations, we address the condition where only one LD is present in the considered network. We believe that this assumption is not far from reality since we expect multiple LDs to occur sequentially, and therefore can be addressed one at a time.

boosting with square loss function, known as least-square boosting (L2Boost), for regression.

Apart from the specific choices of the algorithms, the performance of our solution also depends on the number of samples used to train the machines, n_{TR}. We detail our choice of n_{TR} as well as the number of testing samples, n_{TE}, in Appendix B, followed by a discussion of our strategies to prevent over-fitting of our model in Appendix C.

E. FEATURE SELECTION

For each of the ML tasks, selecting the feature set is crucial for a successful ML performance. We have shown in our prior works [1], [11] that cable degradations cause higher dielectric losses and thus greater attenuation in H_{f} across the frequency band. Therefore, we include the mth-order moments ($m \in \{1, 2, 3, 4\}$) of $|H_{\mathrm{f}}|$ in our feature library to train our machine. Additionally, various studies in the literature, e.g., [11], [20], [40], have shown that degradations reduce the velocity of wave propagation in the degraded section of the cable. Thus, we also include the locations and amplitudes of the peaks in the channel impulse response, h_{f}, and the mth-order moments ($m \in \{1, 2, 3, 4\}$) of $\angle H_{\mathrm{f}}$ in our feature library. Similarly, we also include the mth-order moments ($m \in \{1, 2, 3, 4\}$) of $|H_{\mathsf{ref}}|$ and $\angle H_{\mathsf{ref}}$ in our feature library to provide additional insights for cable health monitoring.

Further, our evaluation results in Figs. 4-6 have also shown that PLM-JTFDR provides cleaner waveforms for extracting features for degradation identification and location, and also indicative information in predicting the LD severity. Therefore, we also extract peak locations and magnitudes from the resultant PLM-JTFDR waveforms as features for our ML operation.

V. SIMULATION RESULTS

In this section, we demonstrate the effectiveness of our ML solution through numerical evaluations for automated cable health condition monitoring. Throughout our simulations, we apply the network topology shown in Fig. 2, and the cable aging model and PLC channel characterization described in Section II and Section III, respectively. In addition, we set $\gamma_{\mathsf{homo}} \sim \mathscr{U}(0, 0.05)$, since the expected lifespan of typical power cables is 30 years [5, Ch. 6], which corresponds to $\gamma_{\mathsf{homo}} = 0.048$ as computed from (1). Further, to clearly distinguish an LD from homogeneous degradation, we vary $\gamma_{\mathsf{local}} \sim \mathscr{U}(0.1, 1)$. Additionally, we use $\ell_{\mathsf{WT}} \sim \mathscr{U}(100, 300)$ m and the center of the localized WT degradation randomly located within 100 m from the center of a branch in Fig. 2. Since n_{TR} and n_{TE} vary for each of the ML tasks, we specify our chosen tuple $(n_{\mathsf{TR}}, n_{\mathsf{TE}})$ with all our results.

A. COOPERATIVE LD IDENTIFICATION

We use the ith PLM, p_i, ($i \in \{1, 2, 3\}$) to identify the presence of a localized WT degradation, regardless of whether it resides between $p_i - \mathsf{BP}$ or $p_i - \mathsf{BE}_i$. For such a task, we use $n_{\mathsf{TR}} = 7000$ and $n_{\mathsf{TE}} = 6600$. Of the 7000 training samples, 1000 are characterized with a homogeneous degradation, and 1000 each with an LD on each of the six branches in the considered network topology shown in Fig. 2. We label the training samples with an LD residing between either $p_i - \mathsf{BP}$ or $p_i - \mathsf{BE}_i$ as *positive*, and the other training samples as *negative*. Thus, we have 2000 positive and 5000 negative training samples. In the testing sample set, for each of the value of γ_{local} between 0 to 1 with a step size of 0.1, we generate 100 samples with an LD located on each of the six branches in the considered network. As a result, for each $\gamma_{\mathsf{local}} \geq 0.1$, we generate 200 positive and 400 negative testing samples. Furthermore, for $\gamma_{\mathsf{local}} = 0$, we generate 600 negative testing samples with a homogeneous degradation.

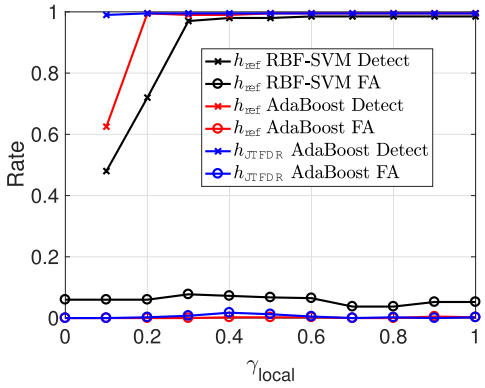

FIGURE 8. Detection and FA rates for cooperative LD identification, with $(n_{\mathsf{TR}}, n_{\mathsf{TE}}) = (7000, 6600)$.

The result of this exercise for varying γ_{local} is shown in Fig. 8. We observe in Fig. 8 that using h_{JTFDR} to extract features provides near-perfect detection with negligible FA rates across all values of γ_{local}, while using h_{ref} provides unsatisfactory detection especially at lower γ_{local}, with either SVM with radial basis function (RBF) kernel or the AdaBoost as our considered ML algorithms. The improved performance is expected due to the nature of h_{JTFDR} in comparison to that of h_{ref}, i.e., more prominent peaks and a smoother floor in h_{JTFDR}, as discussed in Section IV-B. Therefore, the result of Fig. 8 shows that the detection performance can be significantly improved by adopting PLM-JTFDR into the ML framework.

B. LD BRANCH LOCATION

Once a localized WT degradation is detected between $p_i - \mathsf{BP}$ or $p_i - \mathsf{BE}_i$, we let p_j ($j \in \{1, 2, 3\}, j \neq i$) confirm whether the degradation resides between p_i and BP. For such a setting, we generate 2000 *positive* samples with an LD between $p_i - \mathsf{BP}$ and 2000 *negative* samples with an LD between $p_i - \mathsf{BE}_i$, for training the machine. Next, for every γ_{local} between 0.1 to 1 with a step size of 0.1, we generate 200 positive samples with an LD between $p_i - \mathsf{BP}$, and 200 negative samples with an LD between $p_i - \mathsf{BE}_i$, for testing the machine.

The detection results for this phase is shown in Fig. 9. At first, we use the same feature set for this task as that used in the cooperative LD identification. We observe in Fig. 9(a)

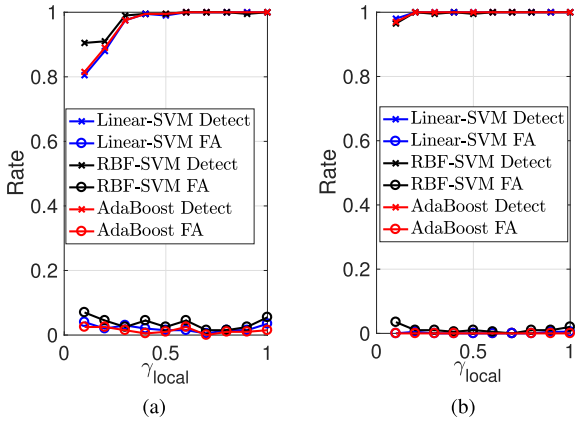

FIGURE 9. Detection and FA rates for LD branch location with (a) the feature set used for Fig. 8, and (b) with optimized features for improved results, both of which are obtained with $(n_{\text{TR}}, n_{\text{TE}}) = (4000, 4000)$.

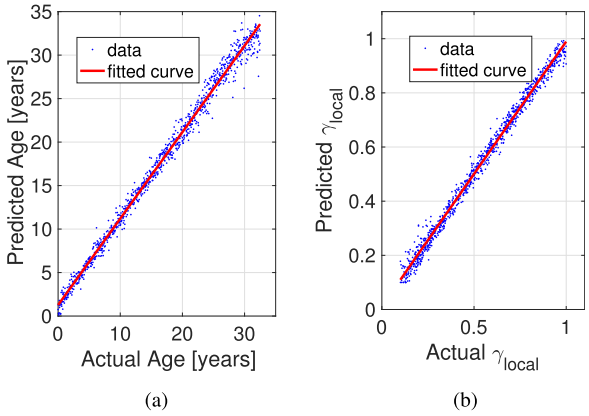

FIGURE 10. Degradation severity assessment with $(n_{\text{TR}}, n_{\text{TE}}) = (3600, 1000)$ for (a) homogeneous aging and (b) LD.

that this results in detection rates that are less than desirable, especially for lower values of γ_{local}. However, by optimizing the selected features, such as using the variance of h_{JTDFR}, the detection rates can be substantially improved across all values of γ_{local}, as seen in Fig. 9(b).

C. HOMOGENEOUS AGING SEVERITY ASSESSMENT

When the aging profile type classification determines a homogeneous aging profile, we use L2Boost to train a machine for the prediction of the degradation severity level. We train and test with different homogeneous degradation severities quantified by their equivalent age as computed in (2). To emulate realistic degradations, we limit $t \sim \mathscr{U}(0, 32.5)$ years in our simulations [5, Ch. 6]. In particular, we use $n_{\text{TR}} = 3600$ with a homogeneous aging and a different set of $n_{\text{TE}} = 1000$. For the homogeneous aging severity assessment, we use the equivalent age computed by γ_{homo} and Equation (2) as the training/testing label.

The equivalent age prediction performance is shown in Fig. 10(a). We observe that the estimated age closely matches the actual age. Furthermore, the prediction accuracy is considerably improved when compared to the state-of-the-art [1], as we now use not only H_{f}, but also H_{ref}. Recall that the equivalent age, t_{eq}, is an intuitive artificial-age indication into the overall degradation severity of the evaluated cable insulation. Therefore, it serves as a reference manifestation of the degradation, where a cable replacement is recommended when the prediction of t_{eq} is nearing or beyond its nominal service lifespan.

D. LD SEVERITY ASSESSMENT

Next, we consider the condition where the classifier indicates the presence of an LD, to assess its severity. To this end, we train an LSBoost regressor with a degradation randomly located anywhere in the TX − BP branch, since we rely on the node closest to the degradation for assessment. We apply $n_{\text{TR}} = 3600$ and $n_{\text{TE}} = 1000$, with training and testing samples each with an LD between TX and BP. For this task, we use γ_{local} as the training/testing label. The prediction results are presented in Fig. 10(b). Similar to the performance gains seen in Section V-C, our results show significant improvement in prediction accuracy when compared to the state-of-the-art [1], due to the additional insight obtained from the waveform of PLM-JTFDR and other features extracted from H_{ref}.

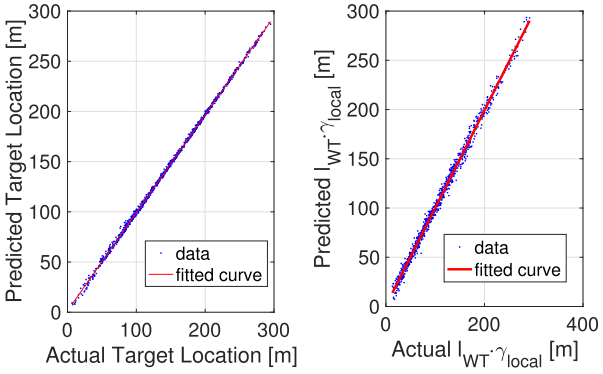

FIGURE 11. LD location results with $(n_{\text{TR}}, n_{\text{TE}}) = (3600, 1000)$ for predicting (a) the target location and (b) the degradation length.

E. LD LOCATION

Thus far, we have predicted the type of degradation present and its severity. As our final diagnostics stage, we attempt to locate the salient localized cable degradation so that further efforts in preventing an in-service fault can be concentrated. Locating an LD consists of determining the positions of its two ends. For this purpose, we follow the procedure of first determining its starting point, or the *target* point, and then estimating the degradation length. For the localization of the target point, we train an SVM for regression with linear kernel. Similar to our choice in Section V-D, we set $n_{\text{TR}} = 3600$ and $n_{\text{TE}} = 1000$, with training and testing samples each with an LD between TX and BP. For this regression task, we use the target location as the training/testing label. The results of predicting the target location can be seen in Fig. 11(a). We notice that the prediction accuracy is near perfect with

negligible variance of individual predictions from the fitted curve. This accurate target location prediction is made possible due to the peak location clarity in h_{JTFDR}.

Next, we predict the length of the degradation to identify its end point. However, we found that the length prediction was highly inaccurate with any ML algorithm or any combinations of extracted features. Therefore, we device a workaround to this challenge by instead predicting the product $\ell_{\mathsf{WT}} \cdot \gamma_{\mathsf{local}}$, which can be predicted with high accuracy, and then using our previously predicted values of γ_{local} (in Fig. 10(b)) to determine ℓ_{WT}. We continue with using $n_{\mathsf{TR}} = 3600$ and $n_{\mathsf{TE}} = 1000$, with training and testing samples each with an LD between TX and BP. Here, we use the product $(\ell_{\mathsf{WT}} \cdot \gamma_{\mathsf{local}})$ as the training/testing label. The prediction results for $\ell_{\mathsf{WT}} \cdot \gamma_{\mathsf{local}}$ is shown in Fig. 11(b), where we clearly notice that the fitted curve of the predictions is a straight line with unit slope and nearly passing through the origin, thereby confirming the high accuracy of our results.

VI. DISCUSSION

In this section, we provide a brief discussion on our proposed solution by comparing it with prior arts and exploring its robustness in non-ideal settings.

A. RELATED WORK

1) REFLECTOMETRY METHODS

Reflectometry methods, such as TDR or JTFDR, are used by utilities for detecting faults and degradations on the line [18], [42]–[44]. While our solution includes the use of the same underlying principle to enhance our proposed ML framework, we synthesize the results of JTFDR using the already existing PLMs that inherently estimate the reflection channel. Therefore, no additional dedicated components are required as in conventional reflectometry methods. Further, by incorporating the reflectometry methods into an ML framework, we are able to comprehensively infer the cable health conditions, which conventional methods are unable to achieve.

2) FAULT LOCATION

Several prior works have proposed and developed solutions to use PLMs for fault detection and location, e.g., [45]–[48]. Apart from these works facing practical limitations, such as, say, requiring a reference CFR measurement for any given load condition, detecting the presence of a fault on the main line is a reactive response to a service failure. In contrast, we develop solutions in our work to estimate cable degradations in order to take preventive measures to avoid a fault. Furthermore, assessing cable degradations is also non-trivial when compared to fault detection as the signal reflections tend to be more obscure [14], also as seen in Fig. 4 and Fig. 5.

3) ML TECHNIQUES

ML-based *data-driven* methods have also been previously used for cable diagnostics, albeit without using PLC. [49] provides a substantial literature review on fault diagnosis using data-driven methods. Further, [40] and [50] also provide techniques to use SVM for cable diagnostics. However, similar to the methods described in Section VI-A.2, these solutions predominantly focus only on fault diagnostics, and also do not involve using PLMs.

4) ALTERNATIVE COMPONENTS FOR DIAGNOSTICS

Fault identification and location methods have been proposed in the literature by using phasor measurement unit (PMU) measurements [51]–[53]. While PMUs are traditionally installed in transmission networks for grid status monitoring, use of distribution-level PMUs or micro-PMUs (μPMUs) has been proposed for distribution networks as well [53], [54]. Nevertheless, the benefits of our solution over such methods are evident. Apart from the added installation cost, the sampling rates and the number of installed μPMUs are insufficient to perform degradation location and severity assessment with the accuracy that we have demonstrated in Section V.

B. ROBUSTNESS TO NON-IDEALITIES

Although the WT model we use in (3) is representative of realistic WT degradations, we explored the robustness of our solution to possible behavior deviations that could be seen in practically encountered WT degradations. Furthermore, typical operation of our method involves training machines offline using synthetically generated channel conditions with degradation models such as (3), and then deploying such machines on PLMs in the real-world. Therefore, we investigate the performance of our solution using practical measurement data as testing samples.

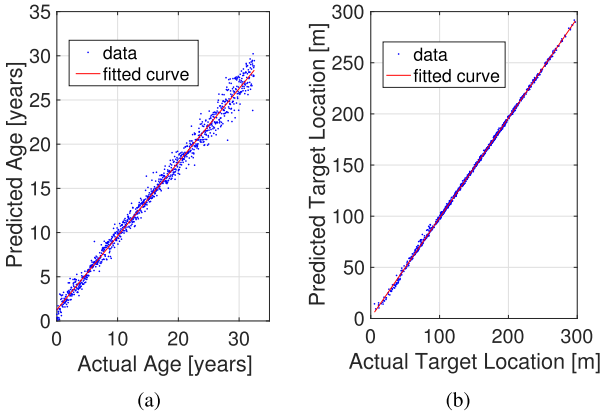

FIGURE 12. Robustness evaluation results of our proposed scheme with $(n_{\mathsf{TR}}, n_{\mathsf{TE}}) = (3600, 1000)$ for (a) predicting the equivalent age of a homogeneous degradation, and (b) the target location for an LD.

To this end, we evaluate our solution by training our machine to associate the behavior of WT degradations with the model of (3), and then testing its performance by applying real-world WT degradation measurements reported in [20, Ch. 6]. The results of this exercise can be seen in Fig. 12. For illustration purposes, we present the result of

two evaluations we performed, one each with and without an LD. First, we predict the equivalent age of a cable that is subject to homogeneous WT degradation. In comparison to similar results obtained earlier in Fig. 10(a), we observe in Fig. 12 that the prediction performance is noticeably affected, as expected. However, our machine is robust enough to provide a satisfactory performance with near unity slope of the fitted line and low individual prediction variance. Next, we focus on analyzing an LD, where we predict its target location, as in Fig. 11(a). In this case, we notice in Fig. 12(b) that the prediction results are still accurate, since locating a degradation mainly relies on the reflection peaks caused due to a discontinuity. The prominent peaks and smooth floor of our proposed PLM-JTFDR make detecting and locating such discontinuities fairly robust to the accuracy of the WT model used.

The framework presented in our work also inspires future engineering endeavors, e.g., investigating the extent of the impact of channel estimation errors on the prediction accuracy, and examining the robustness of our solution when trained with one form of degradation and tested on cables subject to multiple types of degradations and various other non-idealities (e.g., bending of cable or cable splicings).

VII. CONCLUSIONS AND FUTURE WORK

In this paper, we have proposed methods to reuse power line modems available across the smart-grid distribution network to also monitor cable health conditions. We propose a machine learning framework to present an automated cable diagnostics procedure. Our solution includes multiple tasks such as cable aging profile classification, cable degradation severity assessment, and precise degradation location in case of a localized degradation, performed in a sequential manner. Our simulation results show high detection and prediction accuracies for each of these tasks, which can also be attributed to the enhanced features used for machine training that we extract from our newly designed power line modem synthesized joint-time-and-frequency-domain reflectometry technique, as well as to the new insight gained from the reflected channel we use in addition to the end-to-end channel transfer function. The machine uploaded on the power line modems can be updated as often as required with online firmware upgrades. Our proposed technique provides utilities with a low-cost solution that enables them to harness power line modems as not only communication devices, but also as probes to continuously monitor the cable health, which assists in taking preemptive measures to avoid possible cable in-service failures and resultant power outages.

APPENDIX A
PLM-JTFDR

Conventional JTFDR involves transmitting a Gaussian enveloped chirp sequence, $s_{\text{gc}}(t) = g(t) \cdot c(t)$, where $g(t)$ and $c(t)$ are the Gaussian-shaped and the chirp sequences, respectively, and subsequently sampling and processing the reflected signal, $\rho(t)$, to diagnose cable anomalies [18].

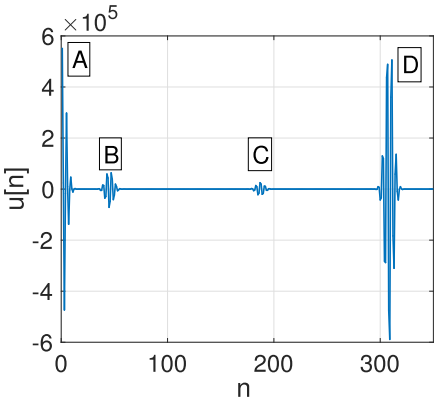

FIGURE 13. The waveform u as computed using (14).

To emulate this procedure in a PLM, we generate $s_{\text{gc}}(t)$, which is sampled and pre-stored in the PLM as $\hat{s}_{\text{gc}}[n]$, where n is the time sample index. We then convolve $\hat{s}_{\text{gc}}$ with the estimated reflected channel impulse response, h_{ref}, to produce the equivalent received JTFDR waveform, $\hat{\rho}$, as

$$\hat{\rho}[n] = (\hat{s}_{\text{gc}} * h_{\text{ref}})[n], \tag{13}$$

where '$*$' indicates the linear convolution operation. Next, we process $\hat{\rho}[n]$ as in conventional JTFDR to obtain locations and magnitudes of peaks in the resultant final waveform, h_{JTFDR}, for detecting and locating any possible cable degradations. Specifically, we first compute the cross-correlation, $u[n]$, as

$$u[n] = \sum_{\delta=-\infty}^{\infty} \hat{s}_{\text{gc}}[\delta]\hat{\rho}[n+\delta]. \tag{14}$$

An example of $u[n]$ is shown in Fig. 13 as synthesized by a PLM when an LD is located between itself and the BP (refer Fig. 2 for the network topology). The reflections from the PLM-line interface, the LD near- and far-ends, and the BP correspond to the denoted points of **A**, **B**, **C**, and **D**, respectively. The high-frequency fluctuations seen around those points hinder accurate detection and location of a potential LD. Therefore, to extract clear and salient peaks caused by each of the discontinuities, we further perform envelope detection on u by passing $u_{\text{mag}}[n] = |u[n]|$ through a low-pass filter to obtain the final PLM-JTFDR waveform as

$$h_{\text{JTFDR}} = f_{\text{LPF}}^{(m)}(u_{\text{mag}}), \tag{15}$$

where $f_{\text{LPF}}^{(m)}(\cdot)$ is the mth order low-pass filter operation. For our use-case, we choose the Butterworth filter implementation, resulting in

$$f_{\text{LPF}}^{(m)}(x)[n] = \left(\mathcal{F}^{-1}\left(H_{\text{BW}}^{(m)}\right) * x\right)[n], \tag{16}$$

for any input signal x, where $\mathcal{F}^{-1}$ is the inverse Fourier transform operator and

$$H_{\text{BW}}^{(m)}(f) = \left(\prod_{k=1}^{m}\left(j\frac{f}{f_c} - e^{\frac{j\pi(2k+m-1)}{2m}}\right)\right)^{-1} \tag{17}$$

is the frequency response of the mth order Butterworth low-pass filter at any frequency f for a 3-dB cut-off frequency f_c, where $j = \sqrt{-1}$. Using a trial-and-error approach, we determine that a 6th order Butterworth filter, i.e., $m = 6$, provides us with sufficient accuracy in h_{JTFDR} to extract features that produce accurate results. We also summarize the operating procedure in Fig. 14.

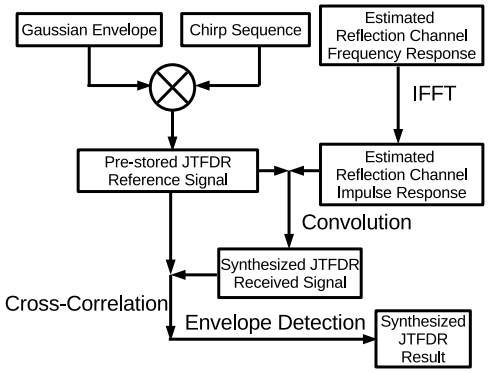

FIGURE 14. Flowchart of PLM-JTFDR following the underlying JTFDR principle outlined in [18].

Since PLM-JTFDR uses the inherently estimated h_{ref}, it does not require any hardware modifications within the PLM. However, additional computations are to be performed digitally in the transceiver chipset to realize (13)–(17).

APPENDIX B
CHOICE OF NUMBER OF TRAINING AND TESTING SAMPLES

As described in Section III, we use the bottom-up approach to simulate BB-PLC channels subject to varying degradation and load conditions as training and testing samples. In such a manner, we independently generate n_{TR} and n_{TE} number of training and testing samples, respectively.

We choose n_{TR} such that the performance of the machine is saturated given a chosen ML algorithm and a specific set of extracted features, and n_{TE} to ensure that we have a sufficient number of testing samples to evaluate the performance of the trained machine to obtain a consistent performance trend in terms of prediction accuracy and prediction variance. Therefore, we choose a large n_{TE} for testing each step of our proposed cable health monitoring scheme. In particular, we choose $n_{\text{TE}} = 1000$ for regression tasks to ensure that a clear trend in the results is observable.

However, the choice of n_{TR} is more intricate. To this end, we present additional numerical results in Figs. 15−17, where the variation in performance of the trained machine with varying n_{TR} for different ML tasks is shown. The performance of LD identification, and degradation severity assessments, for both a homogeneous aging profile as well as an aging profile with an LD, are shown in Figs. 15−17, respectively. We notice that while the performance improves with increasing n_{TR}, it saturates beyond a certain threshold, n_{TH}. n_{TH} is dependent on the ML task, and also on the

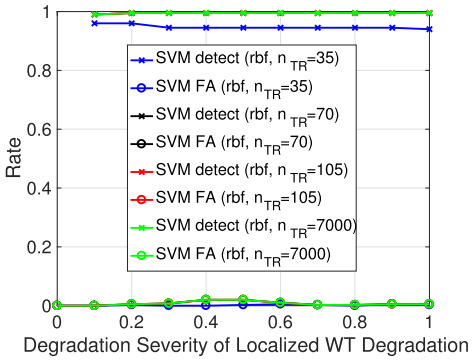

FIGURE 15. Performance of LD identification versus n_{TR}.

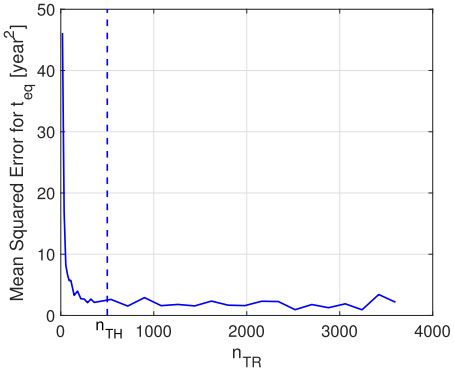

FIGURE 16. Performance of homogeneous degradation severity assessment versus n_{TR}.

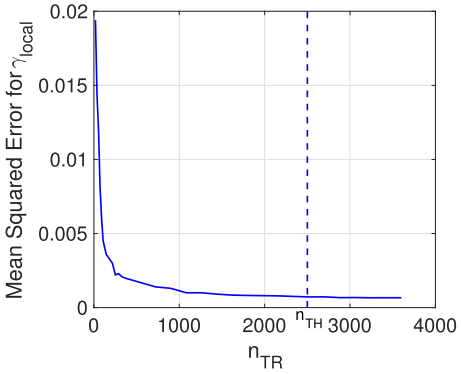

FIGURE 17. Performance of LD severity assessment versus n_{TR}.

channel and network conditions. In our investigations, for the tasks in Figs. 15−17, we have chosen $n_{\text{TR}} = 7000$, $n_{\text{TR}} = 3600$, and $n_{\text{TR}} = 3600$, respectively, which all well-satisfy $n_{\text{TR}} > n_{\text{TH}}$. Specifically, the green curve in Fig. 15, and the far-end points in the blue curves of Figs. 16 and 17 correspond to the performance shown in Fig. 8 (with AdaBoost) and Fig. 10. Similarly, for other tasks presented in our work, we choose a sufficiently large n_{TR} to ensure a saturated performance of the trained machine.

APPENDIX C
STRATEGY TO AVOID OVER-FITTING

The training stage of supervised ML is essentially optimizing the parameters involved in the ML algorithm. When the

parameters of the ML model to be trained are large and the number of training samples is low, the parameters are fitted to the small number of training samples and the trained machine lacks the capability of generalization, i.e., introduces over-fitting. The number of parameters associated with an ML model is closely related to the number of features that we use to train the machine. Typically, ten times the number of features used is the required number of training samples to obtain meaningful results and avoid over-fitting [55]. Since our ML implementation uses at most 16 features, we use at least 3600 training samples ($3600/16 = 225 \gg 10$), and therefore avoid over-fitting. We see from Fig. 15−17, that the performance of the trained machine improves with increasing n_{TR} and saturates beyond a threshold, which is smaller than our chosen n_{TR}.

We note here that we have incurred the difficulty of achieving good results by using a small number of features (at most 16, in our case) in exchange for eliminating risks of over-fitting. When a small number of features is used, we increase the likelihood of encountering conditions where the trained model is not sufficiently comprehensive to predict the label, i.e., we face the issue of under-fitting. In particular, the SVM enforces sparsity on the number of trained support vectors, which determine the boundary for classification or regression. This avoids over-fitting but could result in under-fitting. For some of the tasks, e.g., equivalent age prediction, using an SVM does result in under-fitting. Therefore, we use the boosting technique in such cases, which is able to avoid under-fitting and train a machine with sufficient comprehensiveness to predict the label. In this context, we also note that we use the boosting algorithm for a large portion of our tasks, which is well known to be robust to over-fitting [56]. In such a case, we can simply tune its iteration limit to control the complexity of the trained model and obtain a trained machine that is not subject to over-fitting.

ACKNOWLEDGMENT

This paper was presented at the IEEE International Symposium on Power Line Communications and its Applications (ISPLC), Manchester, U.K., in 2018 [1].

REFERENCES

[1] Y. Huo, G. Prasad, L. Atanackovic, L. Lampe, and V. C. M. Leung, "Grid surveillance and diagnostics using power line communications," in *Proc. IEEE Int. Symp. Power Line Commun. Appl. (ISPLC)*, Apr. 2018, pp. 1–6.

[2] H. Farhangi, "The path of the smart grid," *IEEE Power Energy Mag.*, vol. 8, no. 1, pp. 18–28, Jan./Feb. 2010.

[3] P. Fairley, "Utilities bury more transmission lines to prevent storm damage," *IEEE Spectr.*, vol. 2, pp. 9–10, Jan. 2018. [Online]. Available: https://www.spectrum.ieee.org/energy/the-smarter-grid/utilities-bury-more-transmission-lines-to-prevent-storm-damage

[4] H. Orton, "History of underground power cables," *IEEE Elect. Insul. Mag.*, vol. 29, no. 4, pp. 52–57, Jul. 2013.

[5] P. Gill, *Electrical Power Equipment Maintenance and Testing*. Boca Raton, FL, USA: CRC Press, 2008.

[6] A. Cozza and L. Pichon, "Echo response of faults in transmission lines: Models and limitations to fault detection," *IEEE Trans. Microw. Theory Techn.*, vol. 64, no. 12, pp. 4155–4164, Dec. 2016.

[7] P. B. Andersen *et al.*, *Smart Grid Applications, Communications and Security*. Hoboken, NJ, USA: Wiley, 2012.

[8] V. Dubickas, "On-line time domain reflectometry diagnostics of medium voltage XLPE power cables," Ph.D. dissertation, School Elect. Eng., KTH, Stockholm, Sweden, 2006.

[9] S. Galli, A. Scaglione, and Z. Wang, "For the grid and through the grid: The role of power line communications in the smart grid," *Proc. IEEE*, vol. 99, no. 6, pp. 998–1027, Jun. 2011.

[10] A. Mengi, S. Ponzelar, and M. Koch, "The ITU-T G.9960 broadband PLC communication concept for smartgrid applications," in *Proc. IEEE Int. Conf. Smart Grid Commun. (SmartGridComm)*, Oct. 2017, pp. 492–496.

[11] L. Förstel and L. Lampe, "Grid diagnostics: Monitoring cable aging using power line transmission," in *Proc. IEEE Int. Symp. Power Line Commun. Appl. (ISPLC)*, Apr. 2017, pp. 1–6.

[12] Y. Huo, G. Prasad, L. Lampe, and V. C. M. Leung, "Cable health monitoring in distribution networks using power line communications," in *Proc. IEEE Int. Conf. Commun., Control, Comput. Technol. Smart Grids (SmartGridComm)*, Oct. 2018, pp. 1–6.

[13] L. Yonge *et al.*, "An overview of the HomePlug AV2 technology," *J. Electr. Comput. Eng.*, vol. 2013, Nov. 2013, Art. no. 892628.

[14] L. A. Griffiths, R. Parakh, C. Furse, and B. Baker, "The invisible fray: A critical analysis of the use of reflectometry for fray location," *IEEE Sensors J.*, vol. 6, no. 3, pp. 697–706, Jun. 2006.

[15] T. Neier. (2015). *Cable Diagnostic in MV Underground Cable Networks: Theoretical Background and Practical Application*. [Online]. Available: https://www.pro-test.co.nz/site/pacifictestinstruments/files/PDF/Technical%20Pages/HV%20Cable%20testing%20and%20diagnostic%20Handbook%20.pdf

[16] M. Abou-Dakka, A. Bulinski, S. S. Bamji, and M. Selsjord, "Depolarization current measurements on field-aged XLPE cable insulation," in *Proc. Annu. Rep. Conf. Elect. Insul. Dielectric Phenomena*, Oct. 2008, pp. 21–24.

[17] P. Werelius, "Development and application of high voltage dielectric spectroscopy for diagnosis of medium voltage XLPE cables," Ph.D. dissertation, KTH, Stockholm, Sweden, 2001.

[18] J. Wang, P. E. C. Stone, Y.-J. Shin, and R. Dougal, "Application of joint time-frequency domain reflectometry for electric power cable diagnostics," *IET Signal Process.*, vol. 4, no. 4, pp. 395–405, Aug. 2010.

[19] J.-P. Crine and J. Jow, "A water treeing model," *IEEE Trans. Dielectr. Electr. Insul.*, vol. 12, no. 4, pp. 801–808, Aug. 2005.

[20] G. Mugala, "High frequency characteristics of medium voltage xlpe power cables," Ph.D. dissertation, School Elect. Eng., KTH, Stockholm, Sweden, 2005.

[21] J. Densley, "Ageing mechanisms and diagnostics for power cables—An overview," *IEEE Elect. Insul. Mag.*, vol. 17, no. 1, pp. 14–22, Jan./Feb. 2001.

[22] R. Patsch and J. Jung, "Water trees in cables: Generation and detection," *IEE Proc.-Sci., Meas. Technol.*, vol. 146, no. 5, pp. 253–259, Sep. 1999.

[23] T. L. Hanley, R. P. Burford, R. J. Fleming, and K. W. Barber, "A general review of polymeric insulation for use in HVDC cables," *IEEE Elect. Insul. Mag.*, vol. 19, no. 1, pp. 13–24, Jan./Feb. 2003.

[24] S. Tamboli, S. Mhaske, and D. Kale, "Crosslinked polyethylene," *Indian J. Chem. Technol.*, vol. 11, pp. 853–864, Nov. 2004.

[25] L. A. Pruitt, "Conventional and cross-linked polyethylene properties," in *Total Knee Arthroplasty*. Berlin, Germany: Springer, 2005, pp. 353–360.

[26] W. V. Titow, *PVC PLASTICS: Properties, Processing, and Applications*. Berlin, Germany: Springer, 2012.

[27] F. Stucki, "Dielectric properties and IV-characteristics of single water trees," in *Proc. IEEJ Int. Workshop Electr. Insul.*, Sep. 1993, pp. 7–10.

[28] F. Versolatto and A. M. Tonello, "An MTL theory approach for the simulation of MIMO power-line communication channels," *IEEE Trans. Power Del.*, vol. 26, no. 3, pp. 1710–1717, Jul. 2011.

[29] C. R. Paul, *Analysis of Multiconductor Transmission Lines*. Hoboken, NJ, USA: Wiley, 2008.

[30] F. Gruber and L. Lampe, "On PLC channel emulation via transmission line theory," in *Proc. IEEE Int. Symp. Power Line Commun. Appl. (ISPLC)*, Mar./Apr. 2015, pp. 178–183.

[31] S. Abeysinghe, J. Wu, M. Sooriyabandara, M. Abeysekera, T. Xu, and C. Wang, "Topological properties of medium voltage electricity distribution networks," *Appl. Energy*, vol. 210, pp. 1101–1112, Jan. 2018.

[32] *Devolo A.G. Data Communication in the Medium-Voltage Grid*. Accessed: May 6, 2019. [Online]. Available: https://www.devolo.com/devolo-bpl-modem-mv.html

[33] L. T. Berger, A. Schwager, P. Pagani, and D. Schneider, *MIMO Power Line Communications: Narrow and Broadband Standards, EMC, and Advanced Processing*. Boca Raton, FL, USA: CRC Press, 2014.

[34] HELUKABEL. (2016). *Medium Voltage Power Cables*. [Online]. Available: http://mdmetric.com/prod/helukabel/N.Medium%20Voltage%20Power.pdf
[35] W. Shu, J. Guo, and S. A. Boggs, "Water treeing in low voltage cables," *IEEE Elect. Insul. Mag.*, vol. 29, no. 2, pp. 63–68, Mar./Apr. 2013.
[36] G. Prasad, L. Lampe, and S. Shekhar, "Enhancing transmission efficiency of broadband PLC systems with in-band full duplexing," in *Proc. Int. Symp. Power Line Commun. Appl. (ISPLC)*, Mar. 2016, pp. 46–51.
[37] G. Prasad, L. Lampe, and S. Shekhar, "In-band full duplex broadband power line communications," *IEEE Trans. Commun.*, vol. 64, no. 9, pp. 3915–3931, Sep. 2016.
[38] G. Prasad, L. Lampe, and S. Shekhar, "Digitally controlled analog cancellation for full duplex broadband power line communications," *IEEE Trans. Commun.*, vol. 65, no. 10, pp. 4419–4432, Oct. 2017.
[39] L. G. de Oliveira, M. de L. Filomeno, and M. V. Ribeiro. (2019). "Orthogonal chirp division multiplexing for power line sensing via time-domain reflectometry." [Online]. Available: https://arxiv.org/abs/1901.09923
[40] H. Livani and C. Y. Evrenosoglu, "A machine learning and wavelet-based fault location method for hybrid transmission lines," *IEEE Trans. Smart Grid*, vol. 5, no. 1, pp. 51–59, Jan. 2014.
[41] K. Murphy, *Machine Learning: A Probabilistic Perspective*. Cambridge, MA, USA: MIT Press, 2012. [Online]. Available: https://books.google.ca/books?id=NZP6AQAAQBAJ
[42] Q. Shi, U. Troeltzsch, and O. Kanoun, "Detection and localization of cable faults by time and frequency domain measurements," in *Proc. IEEE Multi-Conf. Syst. Signals Devices*, Jun. 2010, pp. 1–6.
[43] K. W. Burkes, E. B. Makram, and R. Hadidi, "Water tree detection in underground cables using time domain reflectometry," *IEEE Power Energy Technol. Syst. J.*, vol. 2, no. 2, pp. 53–62, Jun. 2015.
[44] C. K. Lee, S. H. Lee, S. J. Chang, J. B. Park, and T. S. Yoon, "Non-invasive monitoring of underground power cables using Gaussian-enveloped chirp reflectometry," *Meas. Sci. Technol.*, vol. 24, no. 10, Sep. 2013, Art. no. 105012.
[45] A. G. Lazaropoulos, "Main line fault localization methodology in smart grid—Part 1: Extended TM2 method for the overhead medium-voltage broadband over power lines networks case," *Trends Renew. Energy*, vol. 3, no. 3, pp. 2–25, 2017.
[46] A. M. Lehmann, K. Raab, F. Gruber, E. Fischer, and R. Müller, and J. B. Huber, "A diagnostic method for power line networks by channel estimation of PLC devices," in *Proc. IEEE Int. Conf. Smart Grid Commun. (SmartGridComm)*, Nov. 2016, pp. 320–325.
[47] F. Passerini and A. M. Tonello, "Full duplex power line communication modems for network sensing," in *Proc. IEEE Int. Conf. Smart Grid Commun. (SmartGridComm)*, Oct. 2017, pp. 1–5.
[48] A. N. Milioudis, G. T. Andreou, and D. P. Labridis, "Detection and location of high impedance faults in multiconductor overhead distribution lines using power line communication devices," *IEEE Trans. Smart Grid*, vol. 6, no. 2, pp. 894–902, Mar. 2015.
[49] S. Ntalampiras, "Fault diagnosis for smart grids in pragmatic conditions," *IEEE Trans. Smart Grid*, vol. 9, no. 3, pp. 1964–1971, May 2018.
[50] J.-A. Jiang *et al.*, "A hybrid framework for fault detection, classification, and location—Part I: Concept, structure, and methodology," *IEEE Trans. Power Del.*, vol. 26, no. 3, pp. 1988–1998, Jul. 2011.
[51] P. Gopakumar, M. J. B. Reddy, and D. K. Mohanta, "Adaptive fault identification and classification methodology for smart power grids using synchronous phasor angle measurements," *IET Gener., Transmiss. Distrib.*, vol. 9, no. 2, pp. 133–145, Jan. 2015.
[52] M. Jamei, A. Scaglione, and S. Peisert, "Low-resolution fault localization using phasor measurement units with community detection," in *Proc. IEEE Int. Conf. Commun., Control, Comput. Technol. Smart Grids (SmartGridComm)*, Oct. 2018, pp. 1–6.
[53] M. Farajollahi, A. Shahsavari, E. Stewart, and H. Mohsenian-Rad, "Locating the source of events in power distribution systems using micro-PMU data," *IEEE Trans. Power Syst.*, vol. 33, no. 6, pp. 6343–6354, Nov. 2018.
[54] H. Mohsenian-Rad, E. Stewart, and E. Cortez, "Distribution synchrophasors: Pairing big data with analytics to create actionable information," *IEEE Power Energy Mag.*, vol. 16, no. 3, pp. 26–34, May/Jun. 2018.
[55] Y. S. Abu-Mostafa. (2012). *Learning From Data*. [Online]. Available: http://work.caltech.edu/telecourse.html
[56] Y. Freund, R. E. Schapire, and N. Abe, "A short introduction to boosting," *J.-Jpn. Soc. Artif. Intell.*, vol. 14, no. 5, pp. 771–780, Sep. 1999.

YINJIA HUO received the M.A.Sc. degree in electrical and computer engineering from The University of British Columbia, Vancouver, BC, Canada, in 2017, where he is currently pursuing the Ph.D. degree with the Department of Electrical and Computer Engineering. His research interests include the power-line communications, the smart grid monitoring, and the applications of machine learning. He was a recipient of the Best Paper Award at the 2018 IEEE International Symposium on Power Line Communications and its Applications (ISPLC).

GAUTHAM PRASAD received the M.S. degree in electrical and computer engineering from the University of Florida, Gainesville, and is approved to receive the Ph.D. degree in electrical and computer engineering from The University of British Columbia, Vancouver, where he is currently a Postdoctoral Research Fellow with the Department of Electrical and Computer Engineering. His research interests broadly include the applications of communication theory, signal processing, and machine learning. He was a recipient of the Best Student Paper Award and the Best Paper Award at the 2018 IEEE International Symposium on Power Line Communications and its Applications (ISPLC).

LAZAR ATANACKOVIC received the B.A.Sc. degree in electrical and computer engineering from The University of British Columbia, Vancouver, BC, Canada, in 2018, where he is currently pursuing the M.A.Sc. degree with the Department of Electrical and Computer Engineering. His research interests span applications in signal processing, machine learning, and communication theory. He was a recipient of the Best Paper Award at the 2018 IEEE International Symposium on Power Line Communications and its Applications (ISPLC).

LUTZ LAMPE (M'02–SM'08) received the Dipl.Ing. and Dr. Ing. degrees in electrical engineering from the University of Erlangen, Germany, in 1998 and 2002, respectively.

Since 2003, he has been with the Department of Electrical and Computer Engineering, The University of British Columbia, Vancouver, BC, Canada, where he is currently a Full Professor. He is a Co-Editor of the book *Power Line Communications: Principles, Standards and Applications from Multimedia to Smart Grid* (John Wiley & Sons, Second Edition, 2016). His research interests include theory and application of wireless, power line, optical wireless, and optical fiber communications.

Dr. Lampe was a (co-)recipient of a number of best paper awards, including awards at the 2006 IEEE International Conference on Ultra-Wideband (ICUWB), the 2010 IEEE International Communications Conference (ICC), and the 2011, 2017, and 2018 IEEE International Conference on Power Line Communications and Its Applications (ISPLC). He was the General (Co-)Chair of the 2005 IEEE ISPLC, the 2009 IEEE ICUWB, and the 2013 IEEE International Conference on Smart Grid Communications (SmartGridComm). He is currently an Associate Editor of the IEEE TRANSACTIONS ON COMMUNICATIONS, the IEEE COMMUNICATIONS LETTERS, and the IEEE COMMUNICATIONS SURVEYS AND TUTORIALS.

VICTOR C. M. LEUNG (S'75–M'89–SM'97–F'03) received the B.A.Sc. degree (Hons.) in electrical engineering from The University of British Columbia (UBC), in 1977, and the Ph.D. degree in electrical engineering from UBC, in 1982, through a Canadian Natural Sciences and Engineering Research Council Postgraduate Scholarship.

From 1981 to 1987, he was a Senior Member of Technical Staff and a Satellite System Specialist with MPR Teltech Ltd., Canada. In 1988, he was a Lecturer with the Department of Electronics, The Chinese University of Hong Kong. He returned to UBC as a Faculty Member, in 1989, and held the positions of Professor and TELUS Mobility Research Chair in Advanced Telecommunications Engineering with the Department of Electrical and Computer Engineering when he retired, in 2018, and became a Professor Emeritus. Since 2019, he has been appointed as a Distinguished Professor with the College of Computer Science and Software Engineering, Shenzhen University, China. He has coauthored more than 1200 journal articles, conference papers, and book chapters and has co-edited 14 book titles. Several of his papers was selected for best paper awards. His research interests are in the broad areas of wireless networks and mobile systems.

Dr. Leung is a Fellow of the Royal Society of Canada, the Engineering Institute of Canada, and the Canadian Academy of Engineering. He received the APEBC Gold Medal as the Head of the 1977 graduating class in the Faculty of Applied Science. He was a Distinguished Lecturer of the IEEE Communications Society. He received the IEEE Vancouver Section Centennial Award, the 2011 UBC Killam Research Prize, the 2017 Canadian Award for Telecommunications Research, the 2018 IEEE TCGCC Distinguished Technical Achievement Recognition Award, and the 2018 ACM MSWiM Reginald Fessenden Award. He coauthored papers that received the 2017 IEEE ComSoc Fred W. Ellersick Prize, the 2017 IEEE Systems Journal Best Paper Award, the 2018 IEEE CSIM Best Journal Paper Award, and the 2019 IEEE TCGCC Best Journal Paper Award. He has served on the editorial boards of the IEEE Journal on Selected Areas in Communications—Wireless Communications Series and Series on Green Communications and Networking, the IEEE Transactions on Wireless Communications, the IEEE Transactions on Vehicular Technology, the IEEE Transactions on Computers, the IEEE Wireless Communications Letters, and the *Journal of Communications and Networks*. He has guest edited many journal special issues and provided leadership to the organizing committees and technical program committees of numerous conferences and workshops. He is serving on the editorial boards of the IEEE Transactions on Green Communications and Networking, the IEEE Transactions on Cloud Computing, the IEEE Access, the IEEE Network, *Computer Communications*, and several other journals. He is named in the current Clarivate Analytics list of Highly Cited Researchers. He is a registered Professional Engineer in the Province of British Columbia, Canada.